Research Square

Preprints are preliminary reports that have not undergone peer review.
They should not be considered conclusive, used to inform clinical practice,
or referenced by the media as validated information.

Deletion of CUL4B in gut epithelium promotes ApcMin/+ adenoma formation by impacting the microenvironment

Beibei Guo
Institute of Molecular Medicine and Genetics
Yawen Zheng
Yujia Fan
Yang Yang
Institute of Molecular Medicine and Genetics
Yuxing Wang
Institute of Molecular Medicine and Genetics
Liping Qin
Yachun An
Xiaoran Xu
Xiyu Zhang
Gongping Sun
Shandong University https://orcid.org/0000-0002-0411-2697
Hao Dou
Changshun Shao
Suzhou Medical College of Soochow University https://orcid.org/0000-0003-2618-9342
Yaoqin Gong
School of Basic Medical Sciences, Cheeloo College of Medicine, Shandong University
https://orcid.org/0000-0001-6871-1560
Baichun Jiang
Shandong University https://orcid.org/0000-0001-5220-1638
Huili Hu (**huhuili@sdu.edu.cn**)
Shandong University

Article

Keywords:

Posted Date: June 26th, 2023

DOI: https://doi.org/10.21203/rs.3.rs-3050354/v1

License: This work is licensed under a Creative Commons Attribution 4.0 International License.
Read Full License

Abstract

Cullin 4B (CUL4B) is a scaffold protein of the E3 ubiquitin ligase complex. Recent studies have reported the converse effect of *CUL4B* in carcinogenesis depending on where it functions. The role of CUL4B in tumor initiation at pre-tumor stage remains unknown. Here we report that CUL4B deficiency in the gut epithelium accelerates $Apc^{Min/+}$ adenoma formation by creating the adenoma-prone immunosuppressive microenvironment. Absence of epithelial CUL4B improves the recruitment and activation of tumor-infiltrating $CD11b^{+}Gr\text{-}1^{+}$ MDSCs. *In vitro* co-culture of MDSCs significantly rescued the reverse phenotype of CUL4B deficient organoids. Mechanistically, CUL4B transcriptionally represses the expression of *Csf3*, one gene encoding secreted chemokine responsible for enrolling MDSCs. Our findings provide an understanding of the interplay between adenoma cells and microenvironment in promoting colorectal cancer (CRC) initiation in the context of activated Wnt.

Introduction

As a scaffold protein of the E3 ubiquitin ligase complex, Cullin 4B (CUL4B) participates in diverse physiological processes [1, 2]. *CUL4B* is overexpressed in multiple tumors. But the effect of *CUL4B* in carcinogenesis seems to depend on where it functions. Knockdown of *CUL4B* in tumor cell lines is proved to suppress tumor proliferation, migration, invasion, sphere formation and capacity of subcutaneous tumorigenesis [3–9]. Meanwhile the reverse effect of CUL4B in immune cells on tumor repressing was also found recently, proving that hematopoietic or myeloid cell-specific deletion of *CUL4B* accelerates carcinogenesis [10, 11]. However, how CUL4B functions in spontaneous adenoma initiation at pre-tumor stage still remains unknown.

Several recent studies have linked the E3 ubiquitin ligase with the tumor microenvironment and myeloid-derived suppressor cells (MDSCs) functions [12, 13]. MDSCs are a heterogeneous group of immature myeloid cells and the chief modulator of immunosuppressive networks under many pathologic conditions including cancer and inflammation. MDSCs are generated in the bone marrow and migrate to the lymphoid organ and tumor site in contribution to the microenvironment and tumor development [14–16]. In mice, MDSCs are characterized by the coexpression of CD11b and Gr-1. Two sub-populations of monocytic and granulocytic groups have been defined [17, 18]. MDSCs inhibit the immune response especially by suppressing T-cell functions [19, 20]. During tumor development, many tumor-cell secreted factors such as tumor-derived granulocyte colony-stimulating factor (G-CSF), granulocyte-macrophage colony-stimulating factor (GM-CSF), macrophage colony-stimulating factor (M-CSF), and stem cell factor, are released in the tumor microenvironment (TME) and stimulate the production or expansion of MDSCs [21]. Proteins such as S100A8 and S100A9 have been reported to play important roles in the generation and recruitment of MDSCs within tumor [22–25].

Colorectal cancer (CRC) is the common malignant tumor with the third incidence and second mortality worldwide [26]. Sequential acquisition of specific genetic changes underlies the progression of stepwise developing CRC [27]. *APC* loss-of-function mutation is the most common event in CRC (80%) that

involving aberrant activation of Wnt/β-catenin signaling and formation of benign polyps [28–30]. MDSCs promote CRC progression by immunosuppression and promoting tumor cell proliferation, stemness, and invasiveness. The increased level of MDSCs in CRC patients has been proved to correlate with reduced survival and therapeutic resistance, suggesting MDSCs as prognostic biomarkers and potential therapeutic targets in CRC [31, 32]. However, it still remains unclear how exactly MDSCs coordinate with tumor cells precisely at the early stage of CRC [33].

In this study we deleted *Cul4b* in gut epithelium in $Apc^{Min/+}$ mice, a preclinical model of inherited CRC. We found that CUL4B limited the progression of adenomatous polyposis. Deletion of CUL4B in gut epithelium altered the adenoma microenvironment by reinforcing the accumulation of MDSCs. Blocking the binding of MDSCs by Ly6G/Ly6C (Gr-1) neutralizing antibody rescued the increased $Apc^{Min/+}$ adenoma formation. *Ex vivo Cul4b* deficient $Apc^{Min/+}$ adenoma organoids lacking immune microenvironment showed a reduction in tumor growth, and co-culture with MDSCs significantly rescued it. Mechanistically, loss of CUL4B transcriptionally increased the expression of secreted proteins G-CSF. Together, our results uncovered a novel mechanism to show how epithelial cells affect immune microenvironment in adenoma promotion, thus providing potential therapeutic targets for CRC.

Results

Conditional deletion of Cul4b in the gut epithelium promotes Apc $^{Min/+}$ adenoma formation

CUL4B was recently identified as a novel regulator of gut self-renewal and intestinal stem cells (ISCs) [34]. To investigate the exact role of CUL4B in initial CRC carcinogenesis, we used the tumor-prone genetic background of $Apc^{Min/+}$ model to assess how CUL4B affected $Apc^{Min/+}$ adenoma formation. We crossed $Apc^{Min/+}$ mice with our previously established *Pvillin-Cre*; $Cul4b^{fn/fn}$ mice [35] to obtain offspring with ($Apc^{Min/+}$; $Cul4b^{\Delta IEC}$) or without ($Apc^{Min/+}$; $Cul4b^{WT}$) *Cul4b* deletion in gut epithelium (Fig. S1A). As expected, significant loss of CUL4B, but not its homologue CUL4A, was confirmed by immunofluorescent staining and immunoblot of $Apc^{Min/+}$; $Cul4b^{\Delta IEC}$ mice (Fig. 1A-1B, Figure S1B-S1C). The immunoblot of remaining expression of CUL4B in knockout tissue was due to its expression in non-epithelial cells. Upon spontaneous loss of the second *Apc* allele, the adenomatous polyposis mutation led to aberrant activation of Wnt signaling and subsequently induced adenoma formation. Unexpectedly, $Apc^{Min/+}$; $Cul4b^{\Delta IEC}$ mice showed an accelerated progress in adenomas formation. An increase in the number of generated adenomas (with the size above 2 mm) was found in both colon and intestinal segments (Fig. 1C-1D, Figure S1D-S1G). Consistently, $Apc^{Min/+}$; $Cul4b^{\Delta IEC}$ mice showed severe splenomegalia and anemia due to increased tumorigenicity (Fig. 1E-1F). Although there is a prone for accelaration of death, no significance was found in survival rate after *Cul4b* deletion (Fig. 1G). The effect of CUL4B loss on adenoma genesis observed in $Apc^{Min/+}$ mice was independent of gender (Fig. 1H). These results suggest that CUL4B deficiency promotes adenoma initiation and progression at the background of $Apc^{Min/+}$.

Inhibition of epithelial CUL4B increases adenoma growth through microenvironment

Loss of heterozygosity (LOH) at the *APC* genetic loci frequently occurs at pre-tumor stage in the majority of human colon cancer [36, 37]. To investigate the underlying cause of increased adenoma development after *Cul4b* deletion, PCR and DNA sequencing were first performed to detect LOH in adenomas from $Apc^{Min/+}$; $Cul4b^{\Delta IEC}$ and control mice using the mismatched primers. The *Apc* allele was deleted in all the adenomas randomly selected from both groups, suggesting that CUL4B deficiency did not affect the LOH (Figure S2A). Meanwhile, no significance was found in cell proliferation and apoptosis within adenomas after the loss of CUL4B (Figure S2B-S2D).

Our previous findings suggest that CUL4B is essential in ISCs self-renewal and regulates the expression of cancer stem cell marker CD44 [3, 34]. As CD44 has been proved as an important regulator of adenoma formation to affect tumor initiation in $Apc^{Min/+}$ mice [38], we detected CD44 expression by immunostaining but only found a slight up-regulation within $Apc^{Min/+}$; $Cul4b^{\Delta IEC}$ adenoma (Figure S2E). Next, *in vitro* epithelial organoids were further generated from $Apc^{Min/+}$; $Cul4b^{\Delta IEC}$ and *control* adenomas as previously reported to investigate the cause of increased adenomas [39–41]. As shown in Fig. 2A and 2B, CUL4B expression was virtually undetectable in $Apc^{Min/+}$; $Cul4b^{\Delta IEC}$ organoids. However, in contrary to *in vivo* phenotype, *Cul4b*-deficient adenomas unexpectedly formed much smaller organoids with a lower formation frequency (Fig. 2C). Meanwhile, the growth speed of re-built *Cul4b*-deficient adenoma organoids during passaging was also significantly reduced (Fig. 2D). In accordance with it, the decreased expression of stem cell markers *Lgr5*, *Sox9*, and *Cd44* was also identified (Fig. 2E). These results revealed the reverse characterizations of CUL4B ablation epithelial cells *in vivo* and *vitro* organoids, suggesting some non-epithelial cells, cell interactions or cell microenvironment are probably responsible for the increased adenoma formation.

Next we performed RNA sequencing (RNA-seq) to get transcriptional profiles of adenomas and adjacent tissues with or without *Cul4b* deletion. 1049, 882 and 360 differentially expressed genes (DEGs, fold change > 2, $p < 0.05$) were identified in adenomas at Stage I (90 days, initiation), Stage II (120 days, progression) and Stage III (150 days, late stage) respectively (Fig. 2F). Meanwhile, 2251, 761 and 312 DEGs were found in the adjacent tissues (Fig. 2F). As CUL4B ablation led to most DEGs at the early phase of $Apc^{Min/+}$ adenoma initiation, gene ontology (GO) analysis of DEGs was only performed in adjacent tissue at Stage I. Multiple immune-related annotations were enriched in $Apc^{Min/+}$; $Cul4b^{\Delta IEC}$ tissues including negative regulation of immune system process and positive regulation of cytokine secretion, suggesting immune microenvironment is altered after *Cul4b* deletion (Fig. 2G).

Accumulation of MDSCs creates tumor-prone microenvironment in Cul4b knockout mice

We next performed flow cytometry and immunostaining to analyze the exact immune cell populations affected in *Cul4b* knockout adenomas. Comparable adenomas with the diameter above 2 mm were analyzed to eliminate the variation caused by tumor size in tumor-infiltrating cells recruitment. The

positive staining of CD45 that representing almost all immunological and hematological cells were comparable between those two groups (Figure S3A). Notably, $CD11b^{+}Gr\text{-}1^{+}$ MDSCs other than other infiltrating immune cell populations were significantly enriched in $Apc^{Min/+}$; $Cul4b^{\Delta IEC}$ adenomas as well as adjacent tissue (NK1.1 staining for NK cells, F4/80 staining for macrophages) (Fig. 3A-3B, Figure S3D-S3E, S3H-S3I). No difference was obseverved in the analysis of cell populations from peripheral blood or spleen (Figure S4B-S4C, S3F-S3G). In order to further confirm the change of MDSCs, CD84, a specific surface marker defining MDSCs, and S100A8 and S100A9, two proteins correlated with activated MDSCs, were elevated in $Apc^{Min/+}$; $Cul4b^{\Delta IEC}$ adenomas (Fig. 3C-3F). As the increase of MDSCs has been associated with repressing T cells [15, 42–45], we further detected the tumor-activated T cells and indeed found a decrease of tumor-infiltrating cytotoxic $CD8^{+}$ T cells (Fig. 3G, Figure S3J). An upregulation of PD-1/PD-L1 expression within $Apc^{Min/+}$; $Cul4b^{\Delta IEC}$ adenomas were also confirmed (Fig. 2H). Taken together, loss of CUL4B promotes the accumulation of MDSCs to create the adenoma permissive microenvironment.

To further confirm the specific effect of MDSC accumulation in accelerating adenoma formation after *Cul4b* deletion, We used anti-mouse Ly6G/Ly6C (Gr-1) neutralizing antibody by intraperitoneal injection. The expression of *Cul4b* was not affected and the function of neutralizing antibody was checked (Fig. 3I-3J). It demonstrated that blockade of Ly6G/Ly6C (Gr-1) reduced adenoma growth and S100A8 expreesion in *Cul4b* deletion mice (Fig. 3K-3L). These results suggest that resisting the function of MDSCs rescued the tumor-prone microenvironment and increased adenoma formation in *Cul4b* knockout mice.

CUL4B inhibits CSF3 expression to prohibit MDSCs recruitment through epigenetic regulation

Many tumor-cell secreted factors such as G-CSF, GM-CSF, interleukins and chemokines, are responsible for recruiting MDSCs [21]. In order to know which secreted protein is changed for MDSCs enrollment in *Cul4b* knockout cells, we performed RT-qPCR to detect the expression of reported chemokines in adenomas. We observed *Csf3*, a gene encoding G-CSF, was increased in *Cul4b*-deficient adenoma (Figure S4A). An elevated expression of *Csf3* was found in both the organoids and isolated $CD44^{+}$ cells (Fig. 4A). Meanwhile, an elevated level of secreted G-CSF was also confirmed in the supernatant by ELISA test (Fig. 4B). Knockdown of *CUL4B* in human HCT116 and murine CT26 cancer cell lines led to obvious increase of G-CSF as well (Fig. 4C-4D). Mechanistically, we next examined whether CUL4B bound to the promoter of *Csf3* gene by quantitative ChIP assay using a series of primers. A binding peak was found at -1561bp to -1338bp upstream of transcription start site (TSS) of *Csf3* promoter (Fig. 4E). Given that CRL4B has been reported to coordinate with PRC2 complex, we further detected the change of histone modification and found that deletion of *Cul4b* resulted in a markedly decrease of the H3K27me3 and H2AK119ub1 at the binding peak, providing the evidence that CUL4B is critical for the transcriptional repression of *Csf3* gene (Fig. 4F).

Ex vivo co-culture with MDSCs reversed decreased growth of $Apc^{Min/+}$; $Cul4b^{\Delta IEC}$ adenoma organoids

To confirm the effect of epithelial loss of CUL4B on MDSCs, we first collected supernatant from comparable number of cultured adenoma organoids with or without *Cul4b* deletion as conditional medium (CM^{WT} or CM^{KO}). Then the migration behavior of wildtype MDSCs treated with either CM^{KO} or CM^{WT} was examined by Transwell migration assays (Figure S4B). As shown in Fig. 5A-5C, an increase of migrated MDSCs and S100A8/9 expression were found after CM^{KO} treatment, suggesting CUL4B-deleted cells improve MDSC migration by soluble factors.

To confirm whether the lack of MDSCs in organoids explains the reverse effect of CUL4B deficiency *in vitro*, we replenished isolated MDSCs into organoid co-culture. Co-culture system was established by growing wildtype or *Cul4b*-deficient organoids on the coated Matrigel with wildtype MDSCs on the upper Transwell (illustrated in Fig. 5D). After 96 hours co-culture, the reduced clony number and size of *Cul4b*-deficient adenoma organoids is obviously rescued (Fig. 5E, Figure S4C). Besides, the decreasing expression of CSC markers (*Cd44* and *c-Myc*) and tumor cell-secreted MDSCs-inducing factors (*Il-6* and *Cox2*) [33, 46–48] was also obviously rescued after co-culture (Fig. 5F). Besides, *ex vivo* co-culture with MDSCs significantly enhanced stemness of *Cul4b* knockout cells and the function of secretion proteins for MDSCs enrollment. These findings above suggest the potential instructive effect of $Apc^{Min/+}$; $Cul4b^{\Delta IEC}$ organoids on MDSCs.

To confirm whether *Cul4b* knockout organoids affected on MDSCs through G-CSF, we interfered *Csf3* by siRNA transfection (Figure S4D-S4F). Treatment with conditional medium collected from organoids after *Csf3* knockdown reduced the increased migration ability and the activated expression of S100A8/9 in $Apc^{Min/+}$; $Cul4b^{\Delta IEC}$ adenoma organoids (Fig. 5G-5I, Figure S4G). Meanwhile, knockdown of *Csf3* in *Cul4b* deficient organoids led to reduced clony number and expression of stem cell markers such as *Cd44* (Fig. 5J-5K). In conclusion, deletion of *CUL4B* led to MDSCs accumulation and activation through transcriptionally derepressing *Csf3* expression.

The correlation of CUL4B and CSF3 expression in CRC patients.

The above results demonstrated that CUL4B restrained the migration of MDSCs to the adenoma microenvironment by suppressing the expression of G-CSF at the early stage of colon adenoma. We further analyzed adenoma clinical databases from The Cancer Genome Atlas (TCGA). *CUL4B* showed a negative correlation with *CSF3* in colorectal adenocarcinoma (COAD) (Fig. 6A), as well as lung adenocarcinoma (LUAD) and prostate adenocarcinoma (PRAD) (Fig. 6B-6C). Indeed, by the cumulative survival analysis of patients, low *CSF3* expression was associated with a prone of increased survival (Fig. 6D). We also analyzed GDS2947 (colorectal adenoma and normal mucosa from 32 patients), a database related to colorectal adenoma formation. As the heatmap showed, CD84, the defined marker of MDSCs, and CCL5, one typical elevated chemokines by MDSCs, were obviously negative correlated with CUL4B expression in adenoma and normal mucosa. While CD44, the stem cell marker was positively correlated (Fig. 6E). The above analysis provided clinical evidence for our findings. In summary, our study reveals that deletion of CUL4B in gut epithelium up-regulates G-CSF expression, thus increases MDSCs recruitment and creates tumor-prone environment, finally promotes $Apc^{Min/+}$ adenoma formation.

Discussion

Tumor initiation including CRC requires a series of genetic and epigenetic alterations that cause uncontrolled tumor cell proliferation and alleviated surveillance of the immune system of eliciting antitumor response. Immune dysfunction occurs to change the tumor microenvironment and the cell-cell interaction between tumor and immune cells [49]. Emerging evidences have highlighted the role of CUL4B in tumor-promotion including its elevated expression and cell proliferation promotion. Meanwhile, deletion of CUL4B in hematopoietic cells exerts opposite tumor-suppressive effect in tumor-bearing mice [10, 11]. Therefore, more studies are required to address the role of CUL4B in tumor initiation especally at early stage.

Here we demonstrate that deletion of CUL4B in gut epithelium accelerates $Apc^{Min/+}$ adenoma formation. First, loss of CUL4B in gut epithelium promotes adenoma formation at the genetic background of Wnt-disturbed *Apc* mutant, recruiting more tumor infiltrating MDSCs and less activated $CD8^+$ T cells. Second, *ex vivo* organoid culture lacking immune cells suggest is adverse to the formation of $Apc^{Min/+}$ adenomas organoids. The addition of MDSCs in the co-cultured assay reverses the decreased capacity of organoid formation and gene expression of *Cd44* and *c-Myc*, emphasizing the reciprocal effect between MDSCs and *CUL4B* deficient epithelial cells in adenoma promotion. Third, we reveal that CUL4B represses the expression of G-CSF, a MDSCs recruiter, by altering the histone modification of its promoter. *Csf3* knockdown in a *Cul4b*-deficient epithelial cells in co-culture system or blockade with Ly6G/Ly6C (Gr-1) neutralizing antibody by intraperitoneal injection rescued the growth of adenoma formation, which totally suggests the effects of CUL4B deletion on $Apc^{Min/+}$ tumorigenesis are due to the accumulation of MDSCs. The analysis of CUL4B, as well as MDSCs relative markers in COAD database from TCGA and GDS2947 support our findings.

MDSCs are a heterogeneous population of immature monocytes and granulocytes identified with the surface expression of the CD11b and Gr-1. MDSCs accumulate in both primary and metastatic tumor sites, where they establish the pro-tumor microenvironment in both immunological and non-immunological methods [50]. Several secreted tumor-derived suppressor factors (TDSFs) have been reported to influence the accumulation of myeloid precursors, such as G-CSF [51, 52], GM-CSF [53] and IL-6 [33]. We observed the upregulation of G-CSF at mRNA level, protein level and secreting level. The tumor G-CSF expression has been proved to be significantly associated with increased MDSCs [52]. Completing MDSCs via anti-mouse Ly6G/Ly6C (Gr-1) antibody administration also enhanced chemosensitivity in G-CSF-producing cervical cancer and endometrial cancer [54, 55]. The classification of tumor-associated neutrophils (TANs) and MDSCs is still unclear due to their similar morphology and markers, indicating we do need to distinguish between TANs and MDSCs. CD84, which was identified as a noval marker defining MDSCs in cancer [56], is enriched in adenoma and adjacent tissue of *Cul4b* depleted mice, providing the domiant role of MDSCs, rather than TANs explains the main change of microenvironment. Whether CUL4B could improve MDSCs-targeting treatment and chemotherapies efficacy of CRC in the background of *Apc* mutation should be further investigated.

CRC is the main cause of global cancer related death. The majority of CRC are initiated by permanent activation of Wnt pathway through *APC* mutation. In our previous research, CUL4B have been proved to contribute to cancer stemness by repressing miR-34a in CRC [3]. Knockdown of *CUL4B*, either in tumor organoids or HCT116 and HT29 cell lines, obviously reduced cell cycle progression and metastasis. Moreover, regardless of CUL4B, MDSCs alone have also been reported to enhance stemness characteristics of ovarian cancer, uterine cervical cancer and breast cancer by increasing cancer cell microRNA101, secreting PEG2 or through IL6/STAT3 and NO/NOTCH cross-talk signaling, respectively [57–59]. In accordance with it, we identified the role of CUL4B in promoting tumor stemness by *ex vivo* culture of $Apc^{Min/+}$ tumor organoids without immune cells. Strikingly, co-cultured with MDSCs significantly reverses the phenotype by upregulating *Il6* and *Cox2*. Not only the colony formation capacity but also the expression of stem cell markers like *Cd44* are greatly increased in $Apc^{Min/+}$; $Cul4b^{\Delta IEC}$ organoids. Proinflammatory S100A8/A9 secreted by tumor and myeloid cells implicate in trafficking of accumulation of MDSCs with an autocrine feedback loop [23]. Transference of exosomal S100A9 of MDSCs have been reported to increase stemness of CRC cells [24]. Indeed, we observe the elevated S100A8/A9 in MDSCs after *ex vivo* co-culture with $Apc^{Min/+}$; $Cul4b^{\Delta IEC}$ organoids. Our findings provide new models for the reciprocal communication between tumor cells and infiltrating immune cells and new evidence to support the important role of immune supervise for tumor driven mutation at the early stage of adenoma formation.

In conclusion, our study reveals a novel function of gut epithelial CUL4B in mouse model of mutated *Apc*-induced tumor initiation and progression by restricting the accumulation of tumor infiltrating MDSCs. Mechanismly, we show that deletion of CUL4B leads to increased expression of G-CSF transcriptionally. Our results suggest the novel role of CUL4B in repressing colon adenoma-permissive microenvironment, providing potential therapeutic strategy to treat CRC.

Materials and methods

Animal experiments

$Apc^{Min/+}$ mice (strain: C57BL/6J, stock number: 002020) and *Pvillin-Cre* mice (strain: C57BL/6J, stock number: T0116) were purchased from Jackson Laboratory and Model Animal Research Center (MARC), respectively. $Cul4b^{fn/fn}$ mice were established by our lab previously (exons 3–5 of the *Cul4b* gene were flanked by loxP sites, which can be recognized by Cre) [35]. We further crossed the $Apc^{Min/+}$ male mice with *Pvillin-Cre*; $Cul4b^{fn/fn}$ female mice to obtain the offsprings. $Apc^{Min/+}$; *Pvillin-Cre*; $Cul4b^{fn/fn}$ ($Apc^{Min/+}$; $Cul4b^{\Delta IEC}$) mice and their control $Apc^{Min/+}$; $Cul4b^{fn/fn}$ ($Apc^{Min/+}$; $Cul4b^{WT}$) mice were used in this study. Genomic DNA was purified from mice tail tips using a standard proteinase kinase digestion method (0.1 mg/ml). Genotyping PCR was used to determine the genotype of the mouse. The primers were listed in Table S1. All animal experiments were carried out with approval of the Animal Care and Use Committee of the School of Basic Medical Science, Shandong University (approval number: KYLL-2017(KS)-363). We did not exclude mice during data statistical analysis, and the included mice were confirmed by testing

knockout efficiency through Western Blot or Immunostaining before processed according to experimental requirements without excessive attrition.

For tumorigenesis evaluation, 4 to 5-month old and genotype-matched mice were randomly selected and analyzed. The entire gastrointestinal tract was excised and separated into the colon and 3 segments of the small intestine: proximal, medial and distal segments. The tissues were washed using cold phosphate buffered saline (PBS) and opened longitudinally. The number and size of adenomas were determined using OLYMPUS SZX16. Venous blood was collected into the anticoagulant tube from mice tails, and the blood routine examination was executed after dilution (10 times) with normal saline. The spleens were obtained, taken pictures and weighed. Murine phenotypes were independent of gender with or without CUL4B deletion. For completed MDSCs, the neutralizing antibody InVivoMAb anti-mouse Ly6G/Ly6C (Gr-1) (Bio X cell, BE0075) and the control antibody InVivoMAb IgG2b (Bio X cell, BE0090) were administered intraperitoneally twice weekly at 100 ug per 20 g in 10 to 12-week mice for 1 month [60, 61].

Organoids culture and viral infection

The adenoma organoids were isolated from adenoma tissue of $Apc^{Min/+}$; $Cul4b^{WT}$ and $Apc^{Min/+}$; $Cul4b^{\Delta IEC}$ mice. Adenoma isolation and cell dissociation were performed as described before [39–41, 62, 63]. Brifely, adenomas were dissected from colon, cutted carefully, washed and digested with 10 mM EDTA at 4°C for 30 min. The cells were seeded in 24-well plates with approximately 10^6 cells per well. Compositions of $Apc^{Min/+}$ adenoma organoids culture medium were listed in the Table S4. The culture medium was refreshed every 2 days and organoids were passaged at a split ratio of 1:3 every 4–7 days. For passaging, organoids were removed from Matrigel by incubating with cell recovery solution (Corning, 354253) on ice for 30 min.

Organoids preparation and viral infection were performed as described before [64]. Adenoma organoids were collected from Matrigel and dissociated into single cells using Trypsin-EDTA (Gibco, 25200072) for 5–15 min at 37°C. After washing and counting, cells were resuspended with infection mixture (lentivirus) and centrifuged in the plate at 500 g for 1h at 32°C. After incubation for 4–6 hours at 37°C, the cells were collected, spun down, resuspended with the mixture of Matrigel and medium, seeded into 24-well plate (Greiner bio-one, GN662102) and cultured.

Co-culture of organoids with MDSCs

MDSCs were isolated with Myeloid-Derived Suppressor Cell Isolation Kit (mouse, Mitenyi Biotec, 130-094-538) from mice spleens according to the manufacturer's instructions. Briefly, a single cell suspension was obtained by digestion, resuspended with PBS buffer (0.5% BSA, 2 mM EDTA, pH7.2) and filtered by tissue grinding and a 30 μm filter. After cell counting, 10^8 cells were used per trial for subsequent processing. After FcR blocking and anti-Ly6G-Biotin incubation, cells were treated with anti-Biotin MicroBeads. Gr-$1^{high}Ly6G^+$ cells were allowed to adsorb on LS column (Mitenyi Biotec, 130-042-401) when the

suspension passed through the MACS separator. Gr-1^{dim}Ly6G^{-} cells were contained in the first flow through fraction and can be magnetically labeled with anti-Gr-1-Biotin and Streptavidin MicroBeads. Immediately flush out the magnetically labeled cells by firmly pushing the plunger into the column and repeat the magnetic separation procedure as described. The purity of MDSCs can reach 90% by using the above Kit of Mitenyi Biotec 130-094-538 in our lab [11].

For co-culture, adenoma organoids were released from Matrigel and dissociated into single cells. After washing and counting, single cells from organoids were seeded into the lower compartment in Matrigel-pre-treated 24-well plates with the concentration of 3x10^4 cells per well. After 6 hours, obtained MDSCs were seeded on the top of the Transwell membrane (Corning, CLS3413) at the ratio of 1:1 according to the method previously described [65].

Conditional medium treatment for MDSCs

For treatment of conditional medium, sterile microscope slides were pre-treated with 1mg/ml poly-lysine at 37°C for 2 hours. MDSCs were isolated and resuspended with conditional medium collected from supernatant of cultured *Apc*$^{Min/+}$; *Cul4b*$^{\Delta IEC}$ and control adenomas (48 hours starting from the same concentration). After incubated for 48 hours, slides were washed by PBS and fixed in ice-cold Immunol Staining Fix Solution (Beyotime, P0098) for 30min. After fixation, the slides were permeabilized by 0.5% TritonX-100 in PBS, blocked for 1 h at room temperature and incubated at 4°C with primary antibodies overnight followed by a secondary antibody. Primary antibody: anti-S100A8 and anti-S100A9. Secondary antibody: anti-rabbit Rhodamine.

BrdU assay

BrdU (Sigma, B9285) solution was intraperitoneally injection into mice with 100 mg/kg [66]. The mice were executed 6 hours after injection and the colon tissues were fixed in 4% PFA overnight and sliced for staining. After antigen retrieval with sodium citrate solution, treated with 2N hydrochloric acid and 0.1 M sodium borate and blocking, slides were incubated with the anti-BrdU (Abcam, ab6326) overnight followed by anti-Rat Rhodamine (Jackson ImmunoResearch, 112-025-003). The slides were observed, and images were captured with OLYMPUS BX51.

Flow cytometry analysis

For immune cells analysis, sufficient single cells were isolated from mice spleen, peripheral blood, colon adjacent and adenoma tissues respectively and incubated with appropriate surface antibodies: anti-CD45-PE/Cy7 (Biolegend, Cat# 103113), anti-CD3-PE/Cy7 (Biolegend, Cat# 100219), anti-CD4-FITC (Invitrogen, 11-0041-85), anti-CD8a-APC (Invitrogen, 47-0081-82), anti-CD11b-FITC (Biolegend, Cat# 101206), anti-Ly6G/Ly6C (Gr-1)-PE (Biolegend, Cat# 108408), anti-CD107a-FITC (Biolegend, Cat# 121605), anti-CD137-APC (Biolegend, Cat# 106109) and anti-CD44-PE (Biolegend, Cat# 103023). For

intracellular staining, cells were treated with Fixation/Permeabilization solution (Invitrogen, 00-5223-56) overnight at 4°C before incubating with intracellular antibodies: anti-IFNγ-PE (Biolegend, Cat# 163503). We defined $CD4^+$ T cells as $CD45^+CD4^+$ $CD8a^-$, $CD8^+$ T cells as $CD45^+CD4^-CD8a^+$, activated $CD4^+$ T as $CD3^+CD4^+CD137^+IFN\gamma^+$ and activated $CD8^+$ T as $CD3^+CD8a^+CD107a^+IFN\gamma^+$ [67, 68]. Data acquisition was performed on Accuri C6 Plus and analyzed via FlowJo (RRID:SCR_008520).

For cell apoptosis, single cells were obtained from adenoma tissue of $Apc^{Min/+}$; $Cul4b^{WT}$ and $Apc^{Min/+}$; $Cul4b^{\Delta IEC}$ mice were measured by PE Annexin V Apoptosis Detection Kit with 7-AAD (Vazyme, A213-01) according to the manufacturer's instructions. The proportion of PE^+ cells were recorded on Accuri C6 Plus and analyzed via FlowJo.

For $CD44^+$ cells sorting of organoids, organoids were digested into single cells and stained using anti-CD44-PE (Biolegend, Cat# 103023) and 7-AAD Viability staining solution (Biolegend, Cat# 420403) for 15 min. The proportion of $PE^+7\text{-}AAD^-$ cells were recorded on BD FACSMelody and analyzed via FlowJo.

Immunostaining

The tissue was fixed in 4% paraformaldehyde (PFA), embedded in paraffin, and sectioned with a thickness of 4 μm. After antigen retrieval with sodium citrate solution and blocking, slides were incubated with primary antibodies over night at 4°C and washed with 0.2% TritonX-100 in PBS followed by a secondary antibody. Primary antibody: anti-CUL4B (Sigma-Aldrich, Cat# C9995), anti-CD45 (Proteintech, 20103-1-AP), anti-Ly6g + Ly6c (Abcam, ab25377), anti-S100A8 (Proteintech, 15792-1-AP), anti-S100A9 (Proteintech, 14226-1-AP), anti-CD44 (Abways, CY5138), anti-F4/80 (Abcam, ab6640), and anti-CD84 (Santa Cruz, sc-23899). Secondary antibody: anti-Rat HRP (Jackson ImmunoResearch, 112-035-003), anti-rabbit HRP (Jackson ImmunoResearch, 111-005-003), anti-Rat Rhodamine (Jackson ImmunoResearch, 112-025-003), anti-rabbit Rhodamine (Jackson ImmunoResearch, 111-025-003) and anti-mouse Fluorescein (Jackson ImmunoResearch, 115-095-003).

Chromatin Immunoprecipitation (ChIP)

ChIP was performed using SimpleChIP® Enzymatic Chromatin IP Kit (Cell Signaling Technology, Cat# 9003). Briefly, 10^7 cells were cross-linked with 1.5% formaldehyde. Then nuclei were collected and chromatin was digested followed by 1–2 μg antibody incubation overnight. After being mixed with magnetic beads for 2 hours, mixtures were washed with low and high salt buffers, and then the DNA was extracted from beads and precipitated. The enrichment of the DNA was analyzed by RT-qPCR using primers specific for target gene promoter [69]. The antibodies for ChIP included CUL4B (Sigma-Aldrich Cat# C9995, RRID: AB_1840781), H2AK119ub1 (Cell Signaling Technology, Cat# 8240S) and H3K27me3 (Cell Signaling Technology, Cat# 9733S).

Statistical analysis

Experimental operation was performed with biological or independent replicates. Statistical analysis was performed using GraphPad Prism upon the unknown information about the genotype. Data significance was analyzed using t test. Bar graphs represented mean ± SEM. P-value < 0.05 was considered statistically significant.

Other methods and materials were provided in supplemental files.

Declarations

Acknowledgments

We sincerely thank Professor Hans Clevers for kindly providing the cell lines to produce recombinant R-spondin1, Noggin and Wnt3a. We thank Professor Bo Han for clinical support. We thank Translational Medicine Core Facility of Shandong University for consultation and instrument availability that supported this work.

This work was supported by the grants from: the National Key R&D Program of China 2019YFA0111400, 2018YFA0507900, the National Natural Science Foundation of China 32122031, 92068121, 31970779, and 31970559, the Funds for Taishan Youth Expert of Shandong Province, Shandong Province National Outstanding Young Scholars Foundation (ZR2021JQ11), Youth Interdisciplinary Innovation Research Group of Shandong University 2020QNQT003 and Key Research and Development Program of Shandong Province (2022CXGC020501).

Author Contributions

H.H., B.J. and Y.G. conceived the project and designed all the experiments. B.G. performed most experiments, Y.A. and L.Q. helped to perform the flow cytometry analysis. X.X., Y.W. and Y.F. provided experimental technical assistance. H.H., Y.Y. and B.G. analyzed the RNA-seq. H.H. and B.G. wrote the manuscript. Y.G., C.S., H.H. and H.D. revised the manuscript.

Competing interests

The authors declare that they have no conflict of interest.

Data Availability Statement

The genomic data (RNA-seq) has been deposited into the Gene Expression Omnibus (GEO) database. Accession number is: GSE189382 (accessible at https://www.ncbi.nlm.nih.gov/geo/query/acc.cgi?acc=GSE189382). All the other datasets and code are available upon request from huhuili@sdu.edu.cn.

References

1. Hannah, J. and P. Zhou, *Distinct and overlapping functions of the cullin E3 ligase scaffolding proteins CUL4A and CUL4B*. Gene, 2015. 573(1): p. 33–45.
2. Kerzendorfer, C., L. Hart, R. Colnaghi, G. Carpenter, D. Alcantara, E. Outwin, et al., *CUL4B-deficiency in humans: understanding the clinical consequences of impaired Cullin 4-RING E3 ubiquitin ligase function*. Mech Ageing Dev, 2011. 132(8–9): p. 366–73.
3. Li, Y., H. Hu, Y. Wang, Y. Fan, Y. Yang, B. Guo, et al., *CUL4B contributes to cancer stemness by repressing tumor suppressor miR34a in colorectal cancer*. Oncogenesis, 2020. 9(2): p. 20.
4. Liu, X., J. Cui, L. Gong, F. Tian, Y. Shen, L. Chen, et al., *The CUL4B-miR-372/373-PIK3CA-AKT axis regulates metastasis in bladder cancer*. Oncogene, 2020. 39(17): p. 3588–3603.
5. Qi, M., M. Jiao, X. Li, J. Hu, L. Wang, Y. Zou, et al., *CUL4B promotes gastric cancer invasion and metastasis-involvement of upregulation of HER2*. Oncogene, 2018. 37(8): p. 1075–1085.
6. Zhao, M., M. Qi, X. Li, J. Hu, J. Zhang, M. Jiao, et al., *CUL4B/miR-33b/C-MYC axis promotes prostate cancer progression*. Prostate, 2019. 79(5): p. 480–488.
7. Hu, H., Y. Yang, Q. Ji, W. Zhao, B. Jiang, R. Liu, et al., *CRL4B catalyzes H2AK119 monoubiquitination and coordinates with PRC2 to promote tumorigenesis*. Cancer Cell, 2012. 22(6): p. 781–95.
8. Yang, Y., R. Liu, R. Qiu, Y. Zheng, W. Huang, H. Hu, et al., *CRL4B promotes tumorigenesis by coordinating with SUV39H1/HP1/DNMT3A in DNA methylation-based epigenetic silencing*. Oncogene, 2015. 34(1): p. 104–18.
9. Duan, P.J., J.H. Zhao, and L.L. Xie, *Cul4B promotes the progression of ovarian cancer by upregulating the expression of CDK2 and CyclinD1*. J Ovarian Res, 2020. 13(1): p. 76.
10. Qian, Y., J. Yuan, H. Hu, Q. Yang, J. Li, S. Zhang, et al., *The CUL4B/AKT/beta-Catenin Axis Restricts the Accumulation of Myeloid-Derived Suppressor Cells to Prohibit the Establishment of a Tumor-Permissive Microenvironment*. Cancer Res, 2015. 75(23): p. 5070–83.
11. Xu, Z., L. Li, Y. Qian, Y. Song, L. Qin, Y. Duan, et al., *Upregulation of IL-6 in CUL4B-deficient myeloid-derived suppressive cells increases the aggressiveness of cancer cells*. Oncogene, 2019. 38(30): p. 5860–5872.
12. Song, G., Y. Zhang, J. Tian, J. Ma, K. Yin, H. Xu, et al., *TRAF6 Regulates the Immunosuppressive Effects of Myeloid-Derived Suppressor Cells in Tumor-Bearing Host*. Front Immunol, 2021. 12: p. 649020.
13. Li, X.M., Z.Y. Zhao, X. Yu, Q.D. Xia, P. Zhou, S.G. Wang, et al., *Exploiting E3 ubiquitin ligases to reeducate the tumor microenvironment for cancer therapy*. Exp Hematol Oncol, 2023. 12(1): p. 34.
14. Talmadge, J.E. and D.I. Gabrilovich, *History of myeloid-derived suppressor cells*. Nat Rev Cancer, 2013. 13(10): p. 739–52.
15. Kumar, V., S. Patel, E. Tcyganov, and D.I. Gabrilovich, *The Nature of Myeloid-Derived Suppressor Cells in the Tumor Microenvironment*. Trends Immunol, 2016. 37(3): p. 208–220.
16. Hegde, S., A.M. Leader, and M. Merad, *MDSC: Markers, development, states, and unaddressed complexity*. Immunity, 2021. 54(5): p. 875–884.

17. Gabrilovich, D.I., *Myeloid-Derived Suppressor Cells*. Cancer Immunol Res, 2017. 5(1): p. 3–8.
18. Gabrilovich, D.I. and S. Nagaraj, *Myeloid-derived suppressor cells as regulators of the immune system*. Nat Rev Immunol, 2009. 9(3): p. 162–74.
19. Tcyganov, E., J. Mastio, E. Chen, and D.I. Gabrilovich, *Plasticity of myeloid-derived suppressor cells in cancer*. Curr Opin Immunol, 2018. 51: p. 76–82.
20. Srivastava, M.K., P. Sinha, V.K. Clements, P. Rodriguez, and S. Ostrand-Rosenberg, *Myeloid-derived suppressor cells inhibit T-cell activation by depleting cystine and cysteine*. Cancer Res, 2010. 70(1): p. 68–77.
21. Veglia, F., M. Perego, and D. Gabrilovich, *Myeloid-derived suppressor cells coming of age*. Nat Immunol, 2018. 19(2): p. 108–119.
22. Sinha, P., C. Okoro, D. Foell, H.H. Freeze, S. Ostrand-Rosenberg, and G. Srikrishna, *Proinflammatory S100 proteins regulate the accumulation of myeloid-derived suppressor cells*. J Immunol, 2008. 181(7): p. 4666–75.
23. Ichikawa, M., R. Williams, L. Wang, T. Vogl, and G. Srikrishna, *S100A8/A9 activate key genes and pathways in colon tumor progression*. Mol Cancer Res, 2011. 9(2): p. 133–48.
24. Wang, Y., K. Yin, J. Tian, X. Xia, J. Ma, X. Tang, et al., *Granulocytic Myeloid-Derived Suppressor Cells Promote the Stemness of Colorectal Cancer Cells through Exosomal S100A9*. Adv Sci (Weinh), 2019. 6(18): p. 1901278.
25. Cheng, P., C.A. Corzo, N. Luetteke, B. Yu, S. Nagaraj, M.M. Bui, et al., *Inhibition of dendritic cell differentiation and accumulation of myeloid-derived suppressor cells in cancer is regulated by S100A9 protein*. J Exp Med, 2008. 205(10): p. 2235–49.
26. Sung, H., J. Ferlay, R.L. Siegel, M. Laversanne, I. Soerjomataram, A. Jemal, et al., *Global Cancer Statistics 2020: GLOBOCAN Estimates of Incidence and Mortality Worldwide for 36 Cancers in 185 Countries*. CA Cancer J Clin, 2021. 71(3): p. 209–249.
27. Akimoto, N., T. Ugai, R. Zhong, T. Hamada, K. Fujiyoshi, M. Giannakis, et al., *Rising incidence of early-onset colorectal cancer - a call to action*. Nat Rev Clin Oncol, 2021. 18(4): p. 230–243.
28. Dow, L.E., K.P. O'Rourke, J. Simon, D.F. Tschaharganeh, J.H. van Es, H. Clevers, et al., *Apc Restoration Promotes Cellular Differentiation and Reestablishes Crypt Homeostasis in Colorectal Cancer*. Cell, 2015. 161(7): p. 1539–1552.
29. Pinto, D. and H. Clevers, *Wnt, stem cells and cancer in the intestine*. Biol Cell, 2005. 97(3): p. 185–96.
30. Su, L.K., K.W. Kinzler, B. Vogelstein, A.C. Preisinger, A.R. Moser, C. Luongo, et al., *Multiple intestinal neoplasia caused by a mutation in the murine homolog of the APC gene*. Science, 1992. 256(5057): p. 668–70.
31. Yin, K., X. Xia, K. Rui, T. Wang, and S. Wang, *Myeloid-Derived Suppressor Cells: A New and Pivotal Player in Colorectal Cancer Progression*. Front Oncol, 2020. 10: p. 610104.
32. Sieminska, I. and J. Baran, *Myeloid-Derived Suppressor Cells in Colorectal Cancer*. Front Immunol, 2020. 11: p. 1526.

33. Weber, R., C. Groth, S. Lasser, I. Arkhypov, V. Petrova, P. Altevogt, et al., *IL-6 as a major regulator of MDSC activity and possible target for cancer immunotherapy*. Cell Immunol, 2021. 359: p. 104254.
34. Fan, Y., X. Huo, B. Guo, X. Zhang, Y. Yang, J. Lian, et al., *Cullin 4b-RING ubiquitin ligase targets IRGM1 to regulate Wnt signaling and intestinal homeostasis*. Cell Death Differ, 2022. 29(9): p. 1673–1688.
35. Jiang, B., W. Zhao, J. Yuan, Y. Qian, W. Sun, Y. Zou, et al., *Lack of Cul4b, an E3 ubiquitin ligase component, leads to embryonic lethality and abnormal placental development*. PLoS One, 2012. 7(5): p. e37070.
36. Luo, L., G.Q. Shen, K.A. Stiffler, Q.K. Wang, T.G. Pretlow, and T.P. Pretlow, *Loss of heterozygosity in human aberrant crypt foci (ACF), a putative precursor of colon cancer*. Carcinogenesis, 2006. 27(6): p. 1153–9.
37. Rowan, A.J., H. Lamlum, M. Ilyas, J. Wheeler, J. Straub, A. Papadopoulou, et al., *APC mutations in sporadic colorectal tumors: A mutational "hotspot" and interdependence of the "two hits"*. Proc Natl Acad Sci U S A, 2000. 97(7): p. 3352–7.
38. Zeilstra, J., S.P. Joosten, M. Dokter, E. Verwiel, M. Spaargaren, and S.T. Pals, *Deletion of the WNT target and cancer stem cell marker CD44 in Apc(Min/+) mice attenuates intestinal tumorigenesis*. Cancer Res, 2008. 68(10): p. 3655–61.
39. Kadosh, E., I. Snir-Alkalay, A. Venkatachalam, S. May, A. Lasry, E. Elyada, et al., *The gut microbiome switches mutant p53 from tumour-suppressive to oncogenic.* Nature, 2020. 586(7827): p. 133–138.
40. Lahde, M., S. Heino, J. Hogstrom, S. Kaijalainen, A. Anisimov, D. Flanagan, et al., *Expression of R-Spondin 1 in Apc(Min/+) Mice Suppresses Growth of Intestinal Adenomas by Altering Wnt and Transforming Growth Factor Beta Signaling*. Gastroenterology, 2021. 160(1): p. 245–259.
41. Cho, Y.H., E.J. Ro, J.S. Yoon, T. Mizutani, D.W. Kang, J.C. Park, et al., *5-FU promotes stemness of colorectal cancer via p53-mediated WNT/beta-catenin pathway activation*. Nat Commun, 2020. 11(1): p. 5321.
42. Mira, E., R.A. Lacalle, J.M. Buesa, G.G. de Buitrago, S. Jimenez-Baranda, C. Gomez-Mouton, et al., *Secreted MMP9 promotes angiogenesis more efficiently than constitutive active MMP9 bound to the tumor cell surface*. J Cell Sci, 2004. 117(Pt 9): p. 1847–57.
43. Toh, B., X. Wang, J. Keeble, W.J. Sim, K. Khoo, W.C. Wong, et al., *Mesenchymal transition and dissemination of cancer cells is driven by myeloid-derived suppressor cells infiltrating the primary tumor*. PLoS Biol, 2011. 9(9): p. e1001162.
44. Yang, L., L.M. DeBusk, K. Fukuda, B. Fingleton, B. Green-Jarvis, Y. Shyr, et al., *Expansion of myeloid immune suppressor Gr + CD11b + cells in tumor-bearing host directly promotes tumor angiogenesis*. Cancer Cell, 2004. 6(4): p. 409–21.
45. Yang, L., J. Huang, X. Ren, A.E. Gorska, A. Chytil, M. Aakre, et al., *Abrogation of TGF beta signaling in mammary carcinomas recruits Gr-1 + CD11b + myeloid cells that promote metastasis*. Cancer Cell, 2008. 13(1): p. 23–35.
46. Sinha, P., V.K. Clements, A.M. Fulton, and S. Ostrand-Rosenberg, *Prostaglandin E2 promotes tumor progression by inducing myeloid-derived suppressor cells*. Cancer Res, 2007. 67(9): p. 4507–13.

47. Rodriguez, P.C., C.P. Hernandez, D. Quiceno, S.M. Dubinett, J. Zabaleta, J.B. Ochoa, et al., *Arginase I in myeloid suppressor cells is induced by COX-2 in lung carcinoma*. J Exp Med, 2005. 202(7): p. 931–9.
48. Bunt, S.K., L. Yang, P. Sinha, V.K. Clements, J. Leips, and S. Ostrand-Rosenberg, *Reduced inflammation in the tumor microenvironment delays the accumulation of myeloid-derived suppressor cells and limits tumor progression*. Cancer Res, 2007. 67(20): p. 10019–26.
49. Bayik, D. and J.D. Lathia, *Cancer stem cell-immune cell crosstalk in tumour progression*. Nat Rev Cancer, 2021. 21(8): p. 526–536.
50. Ouzounova, M., E. Lee, R. Piranlioglu, A. El Andaloussi, R. Kolhe, M.F. Demirci, et al., *Monocytic and granulocytic myeloid derived suppressor cells differentially regulate spatiotemporal tumour plasticity during metastatic cascade*. Nat Commun, 2017. 8: p. 14979.
51. Kowanetz, M., X. Wu, J. Lee, M. Tan, T. Hagenbeek, X. Qu, et al., *Granulocyte-colony stimulating factor promotes lung metastasis through mobilization of Ly6G + Ly6C + granulocytes*. Proc Natl Acad Sci U S A, 2010. 107(50): p. 21248–55.
52. Li, W., X. Zhang, Y. Chen, Y. Xie, J. Liu, Q. Feng, et al., *G-CSF is a key modulator of MDSC and could be a potential therapeutic target in colitis-associated colorectal cancers*. Protein Cell, 2016. 7(2): p. 130–40.
53. Kohanbash, G., K. McKaveney, M. Sakaki, R. Ueda, A.H. Mintz, N. Amankulor, et al., *GM-CSF promotes the immunosuppressive activity of glioma-infiltrating myeloid cells through interleukin-4 receptor-alpha*. Cancer Res, 2013. 73(21): p. 6413–23.
54. Kawano, M., S. Mabuchi, Y. Matsumoto, T. Sasano, R. Takahashi, H. Kuroda, et al., *The significance of G-CSF expression and myeloid-derived suppressor cells in the chemoresistance of uterine cervical cancer*. Sci Rep, 2015. 5: p. 18217.
55. Yokoi, E., S. Mabuchi, N. Komura, K. Shimura, H. Kuroda, K. Kozasa, et al., *The role of myeloid-derived suppressor cells in endometrial cancer displaying systemic inflammatory response: clinical and preclinical investigations*. Oncoimmunology, 2019. 8(12): p. e1662708.
56. Alshetaiwi, H., N. Pervolarakis, L.L. McIntyre, D. Ma, Q. Nguyen, J.A. Rath, et al., *Defining the emergence of myeloid-derived suppressor cells in breast cancer using single-cell transcriptomics*. Sci Immunol, 2020. 5(44).
57. Kuroda, H., S. Mabuchi, E. Yokoi, N. Komura, K. Kozasa, Y. Matsumoto, et al., *Prostaglandin E2 produced by myeloid-derived suppressive cells induces cancer stem cells in uterine cervical cancer*. Oncotarget, 2018. 9(91): p. 36317–36330.
58. Cui, T.X., I. Kryczek, L. Zhao, E. Zhao, R. Kuick, M.H. Roh, et al., *Myeloid-derived suppressor cells enhance stemness of cancer cells by inducing microRNA101 and suppressing the corepressor CtBP2*. Immunity, 2013. 39(3): p. 611–21.
59. Peng, D., T. Tanikawa, W. Li, L. Zhao, L. Vatan, W. Szeliga, et al., *Myeloid-Derived Suppressor Cells Endow Stem-like Qualities to Breast Cancer Cells through IL6/STAT3 and NO/NOTCH Cross-talk Signaling*. Cancer Res, 2016. 76(11): p. 3156–65.

60. Huang, S., Z. Wang, J. Zhou, J. Huang, L. Zhou, J. Luo, et al., *EZH2 Inhibitor GSK126 Suppresses Antitumor Immunity by Driving Production of Myeloid-Derived Suppressor Cells*. Cancer Res, 2019. 79(8): p. 2009–2020.
61. Bodogai, M., K. Moritoh, C. Lee-Chang, C.M. Hollander, C.A. Sherman-Baust, R.P. Wersto, et al., *Immunosuppressive and Prometastatic Functions of Myeloid-Derived Suppressive Cells Rely upon Education from Tumor-Associated B Cells*. Cancer Res, 2015. 75(17): p. 3456–65.
62. Sato, T., D.E. Stange, M. Ferrante, R.G. Vries, J.H. Van Es, S. Van den Brink, et al., *Long-term expansion of epithelial organoids from human colon, adenoma, adenocarcinoma, and Barrett's epithelium*. Gastroenterology, 2011. 141(5): p. 1762–72.
63. Sato, T., R.G. Vries, H.J. Snippert, M. van de Wetering, N. Barker, D.E. Stange, et al., *Single Lgr5 stem cells build crypt-villus structures in vitro without a mesenchymal niche.* Nature, 2009. 459(7244): p. 262-5.
64. Koo, B.K., D.E. Stange, T. Sato, W. Karthaus, H.F. Farin, M. Huch, et al., *Controlled gene expression in primary Lgr5 organoid cultures*. Nat Methods, 2011. 9(1): p. 81–3.
65. Liu, J., P. Li, L. Wang, M. Li, Z. Ge, L. Noordam, et al., *Cancer-Associated Fibroblasts Provide a Stromal Niche for Liver Cancer Organoids That Confers Trophic Effects and Therapy Resistance*. Cell Mol Gastroenterol Hepatol, 2021. 11(2): p. 407–431.
66. Yuan, J., B. Jiang, A. Zhang, Y. Qian, H. Tan, J. Gao, et al., *Accelerated hepatocellular carcinoma development in CUL4B transgenic mice*. Oncotarget, 2015. 6(17): p. 15209–21.
67. Cattaneo, C.M., K.K. Dijkstra, L.F. Fanchi, S. Kelderman, S. Kaing, N. van Rooij, et al., *Tumor organoid-T-cell coculture systems*. Nat Protoc, 2020. 15(1): p. 15–39.
68. Dijkstra, K.K., C.M. Cattaneo, F. Weeber, M. Chalabi, J. van de Haar, L.F. Fanchi, et al., *Generation of Tumor-Reactive T Cells by Co-culture of Peripheral Blood Lymphocytes and Tumor Organoids*. Cell, 2018. 174(6): p. 1586–1598 e12.
69. Lennard Richard, M.L., D. Brandon, N. Lou, S. Sato, T. Caldwell, T.K. Nowling, et al., *Acetylation impacts Fli-1-driven regulation of granulocyte colony stimulating factor*. Eur J Immunol, 2016. 46(10): p. 2322–2332.

Figures

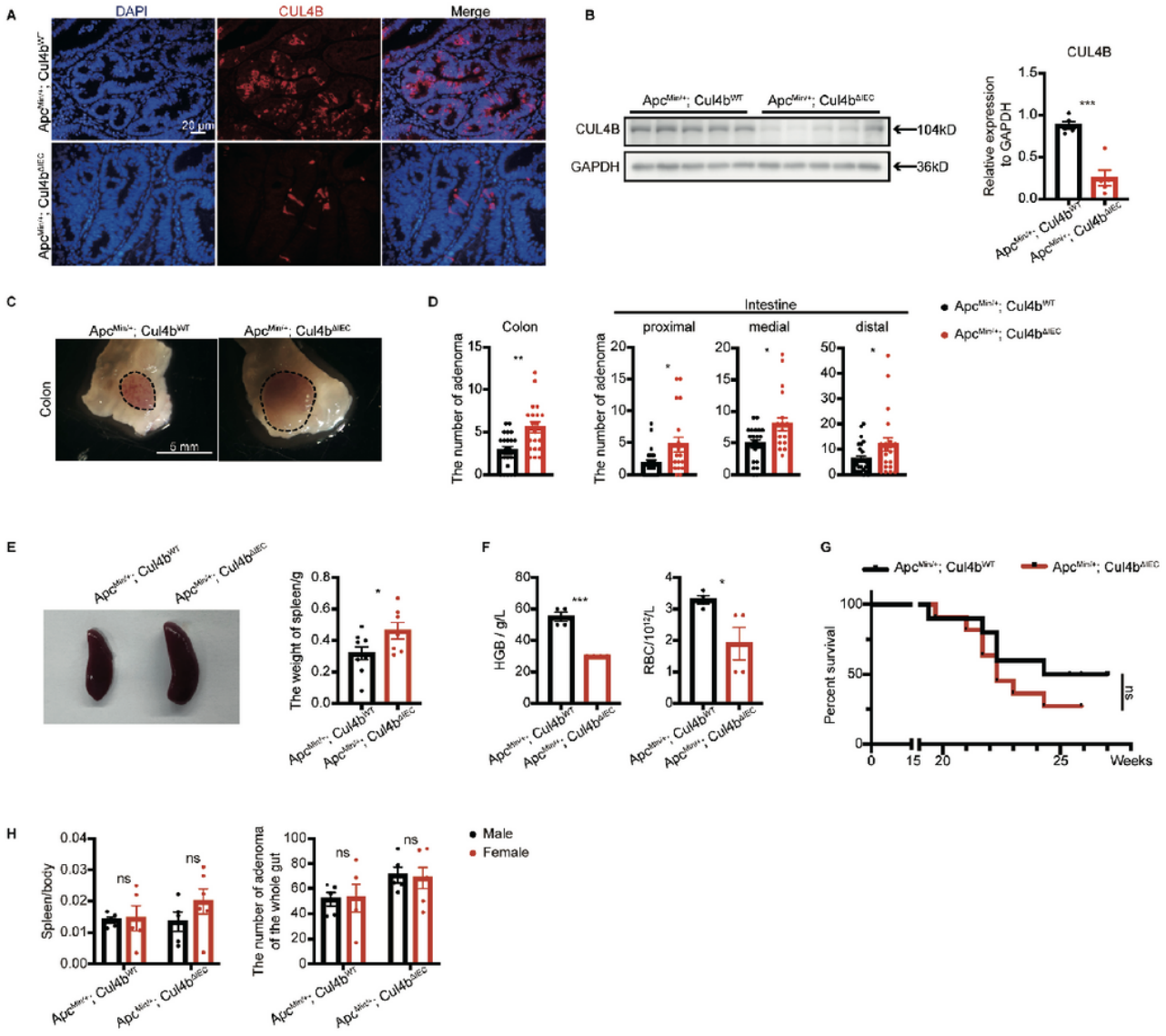


Figure 1

Loss of CUL4B in gut epithelium promotes *Apc*$^{Min/+}$ adenoma formation

(A) The representative images of immunofluorescent staining of CUL4B in adenomas of *Apc*$^{Min/+}$; *Cul4b*$^{\Delta IEC}$ (n=3) and *Apc*$^{Min/+}$; *Cul4b*^{WT} mice (n=3). Red, CUL4B; Blue, DAPI. **(B)** Western Blot analysis of CUL4B to detect the knockout efficiency in *Apc*$^{Min/+}$; *Cul4b*$^{\Delta IEC}$ mice (n=5) with GAPDH as the reference. **(C)** The representative images of the adenomas from *Apc*$^{Min/+}$; *Cul4b*$^{\Delta IEC}$ (n=9) and *Apc*$^{Min/+}$; *Cul4b*^{WT} mice (n=9). Dotted lines indicate adenomas in colon. **(D)** Total number of the adenomas with the size >2 mm in proximal, medial and distal segments of intestine and colon from *Apc*$^{Min/+}$; *Cul4b*$^{\Delta IEC}$ (n=9) and *Apc*$^{Min/+}$; *Cul4b*^{WT} mice (n=9). All mice were 5-month-old. **(E)** The representative images and statistical analysis of the spleen weight of *Apc*$^{Min/+}$; *Cul4b*$^{\Delta IEC}$ mice (n=7) and *Apc*$^{Min/+}$; *Cul4b*^{WT} mice (n=9). **(F)** The examination of peripheral blood collected from *Apc*$^{Min/+}$; *Cul4b*$^{\Delta IEC}$ mice (n=4) and *Apc*$^{Min/+}$; *Cul4b*^{WT}

mice (n=4). **(G)** Kaplan-Meier survival analysis of *Apc*$^{Min/+}$; *Cul4b*$^{\Delta IEC}$ mice (n=11) and *Apc*$^{Min/+}$; *Cul4b*^{WT} mice (n=10). **(H)** The spleen weight (left) and numbers of adenomas in the whole gut (right) were analyzed in grouped male and female mice of *Apc*$^{Min/+}$; *Cul4b*$^{\Delta IEC}$ and *Apc*$^{Min/+}$; *Cul4b*^{WT}. Data are expressed as the mean ± SEM. p-values *<0.05, **<0.01, ***<0.001, ns, not significant.

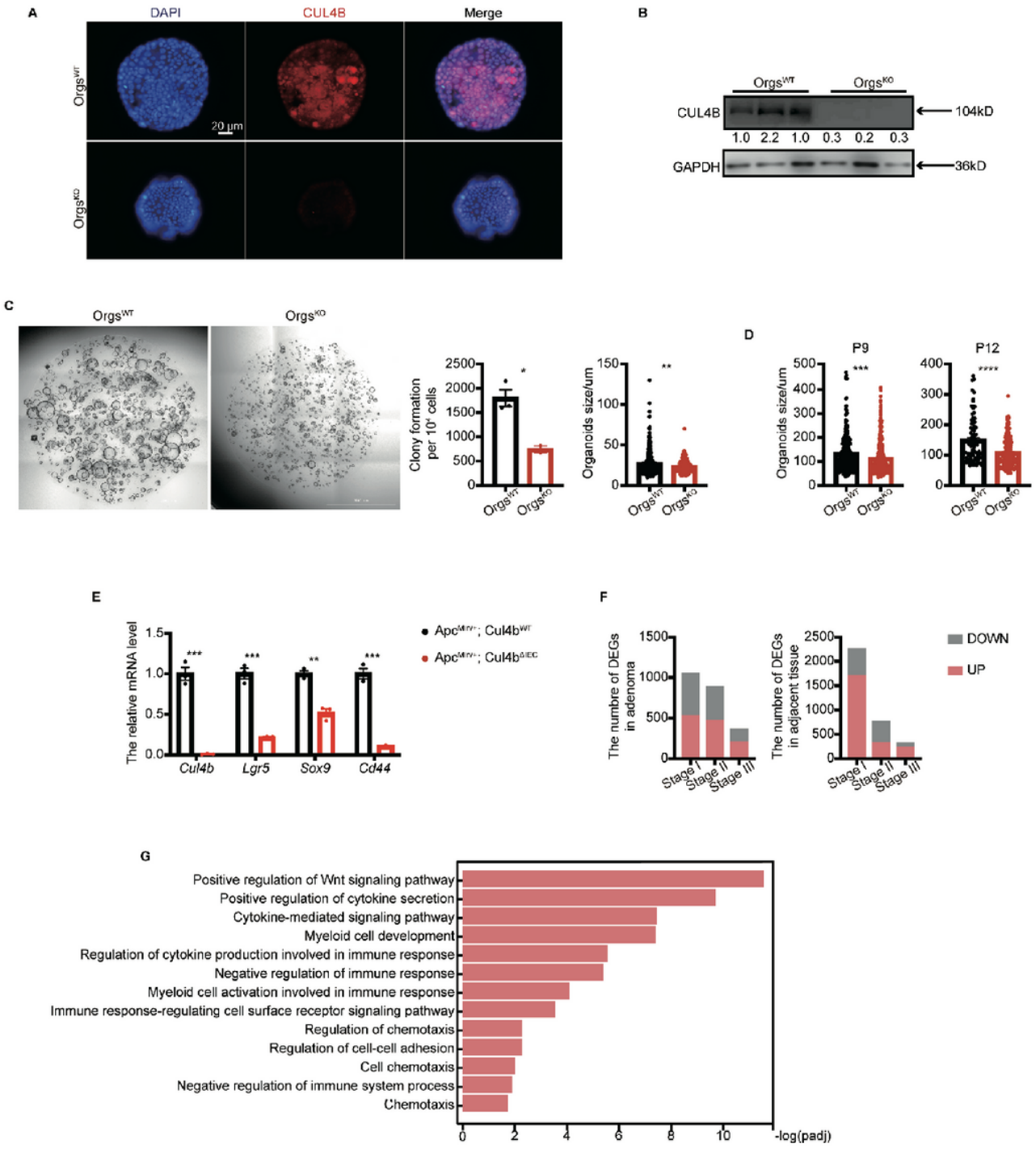


Figure 2

Cul4b deficiency reduces *in vitro* organoids formation of $Apc^{Min/+}$ adenomas through immune microenvironment

(A) The representative images of immunofluorescent staining of CUL4B in adenoma organoids from $Apc^{Min/+}$; $Cul4b^{\Delta IEC}$ ($Orgs^{KO}$, n=3) and $Apc^{Min/+}$; $Cul4b^{WT}$ ($Orgs^{WT}$, n=3). Red, CUL4B; Blue, DAPI. **(B)** Western Blot analysis to detect the knockout efficiency of CUL4B in $Orgs^{WT}$ (n=3) and $Orgs^{KO}$ (n=3). **(C)** The representative images in the bright field (Left) and statistical analysis (right) of adenoma organoids formation and size of $Orgs^{WT}$ (n=3) and $Orgs^{KO}$ (n=5). **(D)** The size of $Orgs^{WT}$ and $Orgs^{KO}$ at passage 9 and 12 was compared by single cell assay. Three independent experiments were performed with triplicate wells. **(E)** The mRNA level of *Lgr5*, *Sox9* and *Cd44* in $Orgs^{WT}$ and $Orgs^{KO}$. Three independent experiments were performed with triplicate wells. **(F)** The statistical analysis the number of DEGs in adenoma and adjacent tissue from Stage I, Stage II and Stage III mice. **(G)** GO analysis of DEGs identified by RNA-seq from $Apc^{Min/+}$; $Cul4b^{\Delta IEC}$ and $Apc^{Min/+}$; $Cul4b^{WT}$ mice at stage I. Data are expressed as the mean ± SEM. p-values *<0.05, **<0.01, ***<0.001, ****<0.0001.

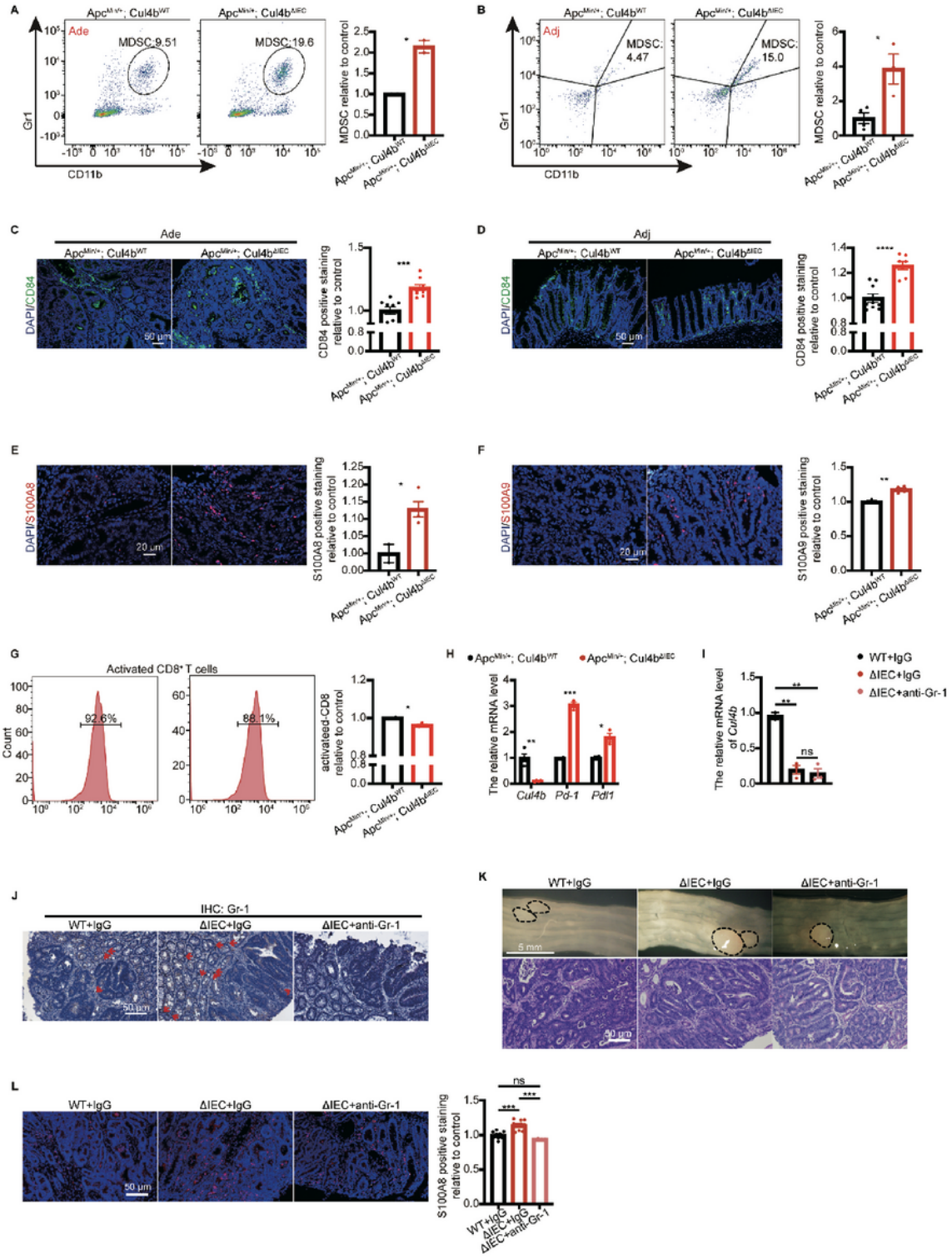


Figure 3

Epithelial loss of CUL4B regulates adenoma progression by recruiting more MDSCs

(A-B) The flow cytometry analysis of $CD11b^{+}Gr\text{-}1^{+}$ MDSCs in adenomas (**A**, 2vs2) and adjacent normal tissues (**B**, 4vs3) from *Apc*$^{Min/+}$; *Cul4b*$^{\Delta IEC}$ and *Apc*$^{Min/+}$; *Cul4b*^{WT} mice. **(C-D)** The representative images and statistical analysis of immunostaining of MDSCs marker CD84 in adenoma (**C**, 2vs2) and adjacent

tissue (**D**, 2vs2) from *Apc*$^{Min/+}$; *Cul4b*$^{\Delta IEC}$ and *Apc*$^{Min/+}$; *Cul4b*^{WT} mice. Green, CD84; Blue, DAPI. **(E-F)** The representative images and statistical analysis of immunostaining of S100A8 (**E**, 2vs4) and S100A9 (**F**, 3vs4) in adenoma from *Apc*$^{Min/+}$; *Cul4b*$^{\Delta IEC}$ and *Apc*$^{Min/+}$; *Cul4b*^{WT} mice. Red, S100A8/S100A9; Blue, DAPI. **(G)** The flow cytometry analysis of activated CD8^{+} T cells within adenoma from *Apc*$^{Min/+}$; *Cul4b*$^{\Delta IEC}$ (n=3) and *Apc*$^{Min/+}$; *Cul4b*^{WT} (n=2) mice. **(H)** The mRNA level of *Pd1* and *Pdl1* in adenoma of *Apc*$^{Min/+}$; *Cul4b*$^{\Delta IEC}$ and *Apc*$^{Min/+}$; *Cul4b*^{WT} mice identified by RT-qPCR. **(I)** The knockout efficiency of *Cul4b* before and after processing with neutralizing antibody using RT-qPCR (2vs3vs3). **(J)** The representative images and statistical analysis of immunochemical staining of Ly6G/Ly6C(Gr-1) to detect the blocking efficiency (2vs3vs3). Red arrows indicate positive staining. **(K)** The representative images of the adenomas (upper) and the sections stained by (H&E) (lower) of adenomas from WT+IgG (n=2), ΔIEC+IgG (n=3) and ΔIEC+anti-Ly6G/Ly6C (Gr-1) (n=3) mice. Dotted lines indicate adenomas in colon. **(L)** The representative images and statistical analysis of immunofluorescent staining of S100A8 of adenoma in WT+IgG (n=2), ΔIEC+IgG (n=3) and ΔIEC+anti-Ly6G/Ly6C (Gr-1) (n=3) mice. Data are shown as the mean ± SEM. p-values *<0.05, **<0.01, ***<0.001, ****<0.0001, ns, not significant.

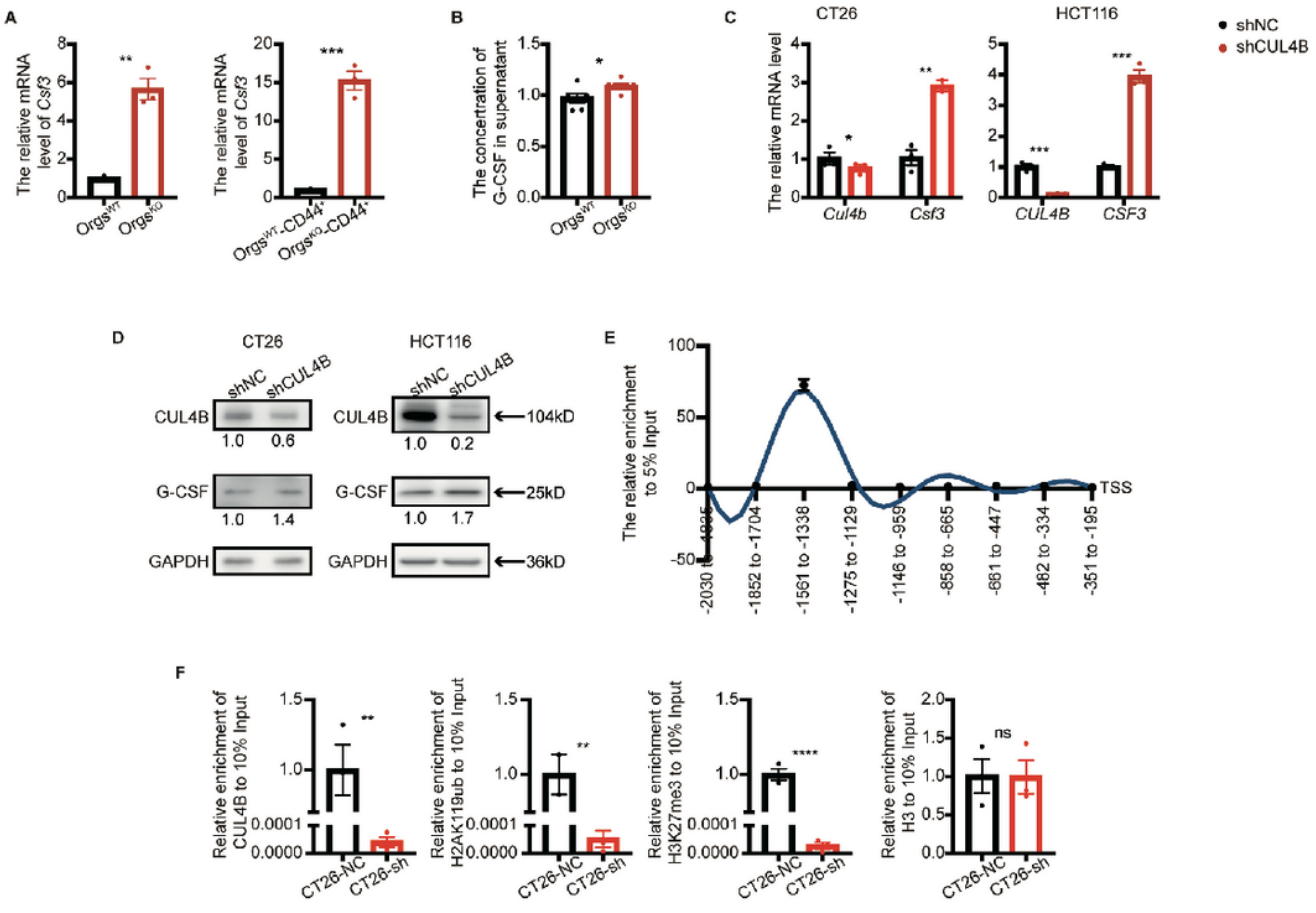


Figure 4

CUL4B inhibits the accumulation and activation of MDSCs through transcriptional repressing of G-CSF

(A) The mRNA level of *Csf3* in the Orgs^{KO} and Orgs^{WT} and in the the organoids of Orgs^{KO} and Orgs^{WT} derived from sorted CD44^{+} cells. **(B)** ELISA analysis of secreted G-CSF in the collected cell supernatant with the same cell number from Orgs^{WT} (n=3) and Orgs^{KO} (n=3). Three independent experiments were performed with triplicate wells. **(C, D)** The protein (**C**) and mRNA level (**D**) of G-CSF in the CUL4B deficient and control murine CT26 and human HCT116 cells. Three independent experiments were performed. **(E)** qPCR after ChIP was performed to check the binding of CUL4B to *Csf3* promoter by using a series of primers. Three independent experiments were performed. **(F)** qPCR after ChIP was performed in wildtype and CUL4B ablation CT26 cells to check the changes of CUL4B, H2AK119ub, H3K27me3 associated with the *Csf3* promoter (-1561bp to -1338bp) with Histone 3 as the control. Three independent experiments were performed. Data are shown as the mean ± SEM. p-values *<0.05, **<0.01, ***<0.001, ****<0.0001, ns, not significant.

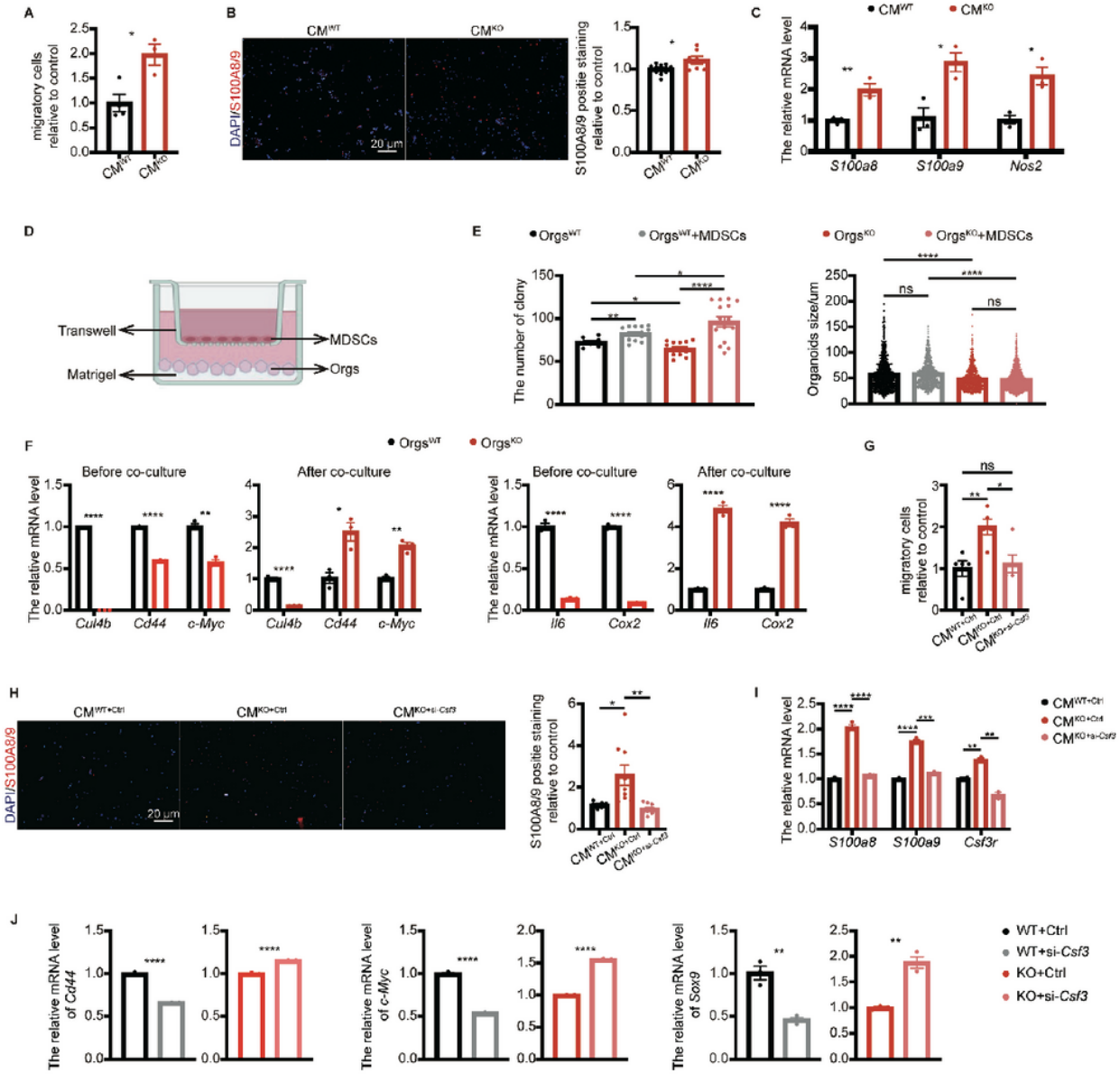


Figure 5

Ex vivo co-culture strengthens MDSC migration and rescues the phenotype of *Apc*$^{Min/+}$; *Cul4b*$^{\Delta IEC}$ adenoma organoids

(A) Calculation of migrated MDSCs in the migration assay treated with CM^{WT} and CM^{KO} for 3 hours. Four independent experiments were performed. **(B)** The representative images and statistical analysis of immunofluorescent staining of S100A8/9 of MDSCs treated with CM^{WT} and CM^{KO} for 48 hours that from comparable number of cultured adenoma organoids with or without *Cul4b* deletion. Red, S100A8/9; Blue, DAPI. Three independent experiments were performed. **(C)** The mRNA level of *S100a8*, *S100a9* and *Nos2* of MDSCs treated with CM^{WT} and CM^{KO} for 72 hours identified by RT-qPCR. **(D)** Illustration of co-culture of wildtype MDSCs and GFP-labeled $Orgs^{WT}$ and $Orgs^{KO}$. **(E)** The number of clony formation (left) and organoids size (right) of $Orgs^{WT}$ and $Orgs^{KO}$ after co-culture. Three independent experiments were performed. **(F)** The mRNA expression of CSC markers (left) (*Cd44* and *c-Myc*) and tumor secreted factors (right) (*Il6* and *Cox2*) in $Orgs^{WT}$ and $Orgs^{KO}$ before and after co-culture. **(G)** Calculation of migrated MDSCs in the migration assay treated with $CM^{WT+Ctrl}$, $CM^{KO+Ctrl}$ and $CM^{KO+si\text{-}Csf3}$ by counting. Three independent experiments were performed. **(H)** The statistical analysis of immunofluorescent staining of S100A8/9 of MDSCs treated with $CM^{WT+Ctrl}$, $CM^{KO+Ctrl}$ and $CM^{KO+si\text{-}Csf3}$. Three independent experiments were performed. **(I)** The mRNA level of *S100a8*, *S100a9* and *Csf3r* of MDSCs treated with $CM^{WT+Ctrl}$, $CM^{KO+Ctrl}$ and $CM^{KO+si\text{-}Csf3}$ for 48 h identified by RT-qPCR. **(J)** The statistics of colony formation number (left) and organoids size (right) of pre-knockdown *Csf3* organoids after 96 h co-culture. Three independent experiments were performed. **(K)** The mRNA level of stem cell markers *Cd44*, *c-Myc* and *Sox9* of pre-knockdown *Csf3* organoids from *Apc*$^{Min/+}$; *Cul4b*$^{\Delta IEC}$ and *Apc*$^{Min/+}$; *Cul4b*^{WT} mice after 96 h co-culture by RT-qPCR. Data are shown as the mean ± SEM. p-values *<0.05, **<0.01, ***<0.001, ****<0.0001, ns, not significant.

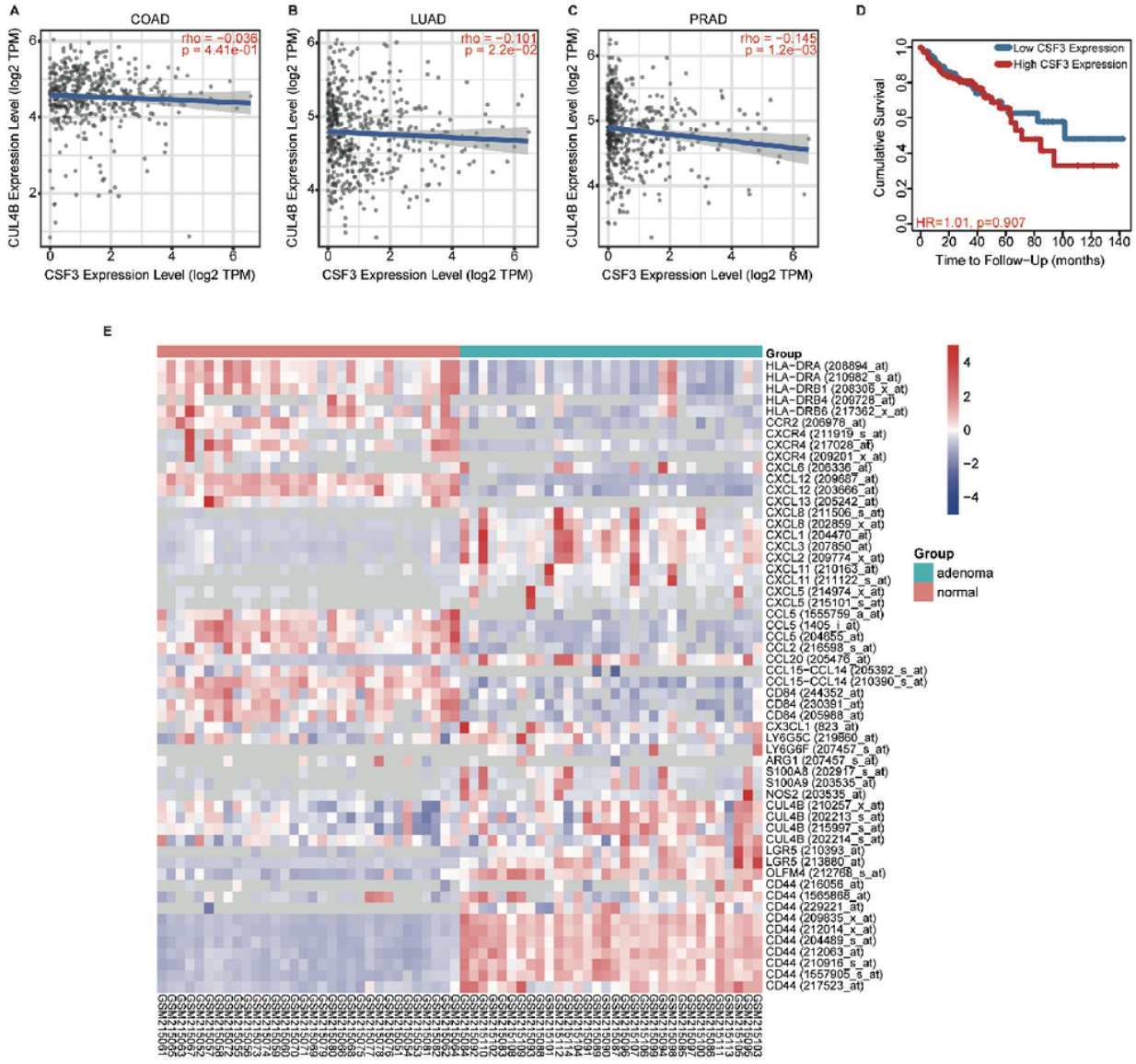


Figure 6

Negative correlation between CUL4B and CSF3 expression in multiple types of adenoma

(A-C) The Spearman correlation analysis of the expression of CUL4B and CSF3 in COAD (**A**), LUAD (**B**) and PRAD (**C**) in TCGA. **(D)** The cumulative survival analysis related to the expression of CSF3 in COAD. **(E)** The heatmap of genes related to MDSCs in GDS2974 using bioinformatic analysis. **(F)** Graphic summary of our research.

Supplementary Files

This is a list of supplementary files associated with this preprint. Click to download.

- SupplementaryInformationoncogenesis.pdf
- GraphicalAbstract.png